

Article pubs.acs.org/JACS

Patchy Colloidal Clusters with Broken Symmetry

You-Jin Kim, $^{\nabla}$ Jae-Hyun Kim, $^{\nabla}$ In-Seong Jo, David J. Pine, Stefano Sacanna, and Gi-Ra Yi *



Cite This: J. Am. Chem. Soc. 2021, 143, 13175-13183



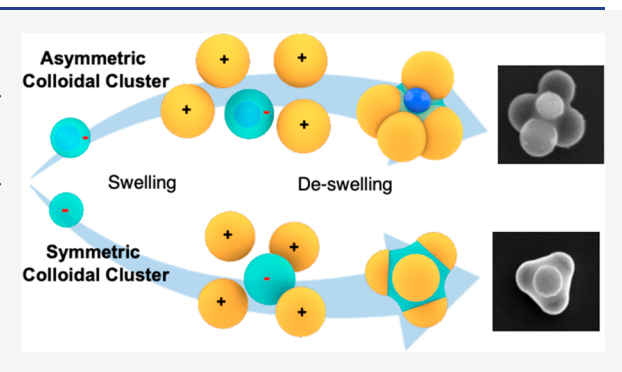
ACCESS I

Metrics & More

Article Recommendations

Supporting Information

ABSTRACT: Colloidal clusters are prepared by assembling positively charged cross-linked polystyrene (PS) particles onto negatively charged liquid cores of swollen polymer particles. PS particles at the interface of the liquid core are closely packed around the core due to interfacial wetting. Then, by evaporating solvent in the liquid cores, polymers in the cores are solidified and the clusters are cemented. As the swelling ratio of PS cores increases, cores at the center of colloidal clusters are exposed, forming patchy colloidal clusters. Finally, by density gradient centrifugation, high-purity symmetric colloidal clusters are obtained. When silica-PS core-shell particles are swollen and serve as the liquid cores, hybrid colloidal clusters are obtained in which each silica nanoparticle is relocated to the liquid core interface during the swelling-



deswelling process breaking symmetry in colloidal clusters as the silica nanoparticle in the core is comparable in size with the PS particle in the shell. The configuration of colloidal clusters is determined once the number of particles around the liquid core is given, which depends on the size ratio of the liquid core and shell particle. Since hybrid clusters are heavier than PS particles, they can be purified using centrifugation.

1. INTRODUCTION

Colloidal particles have been extensively investigated as model systems for understanding the dynamics of atomic structures.¹⁻⁷ They have also been used as building blocks for building up structured materials by self-assembly, of which superstructures show unique optical, acoustic, or mechanical properties due to strong resonant interaction with waves. 1,8-11 Recently, for understanding the dynamics of complex biomolecules like proteins, unconventional colloidal particles with anisotropic shapes or interactions were proposed and explored heavily in simulations for over two decades. 12-18 Colloidal clusters, introduced experimentally in 2003, 19 have received a great deal of attention as a new three-dimensional element for self-assembled colloidal superstructures. 6,20-24 Later, they were partially encapsulated with polymers in the seeded polymerization process producing patchy particles, which can be used to form complex superstructures as biomolecules do.25 Computational simulations have also been extensively used to explore and predict colloidal superstructures of colloidal clusters or patchy particles^{26–31} and through multistep assembly of Janus particles. 32-34

DNA was selectively coated on their patches, which led to programmable colloidal molecules or atoms. Recently, highdensity DNA brushes were coated on colloids in several ways, which resulted in various programmed colloidal superstructures including face-centered cubic, CsCl-like, and AlB2like structures.³⁵⁻³⁹ More importantly, colloidal clusters were successfully coassembled with colloidal spheres, which formed a new class of colloidal phases through the selective DNA hybridization. In particular, tetrahedral clusters and spheres can form the MgCu₂ Laves structure, which is made up of interpenetrating diamond and pyrochlore sublattices. 40 Both open sublattices exhibit large full photonic bandgaps, which is critical in the further development of optical devices. 41-43

The emulsion-assisted method developed for colloidal clusters 19 has been further developed for plasmonic clusters of metal nanoparticles 46 and soft patchy particles of block copolymers. 47,48 However, these methods are multistep processes and require a post separation process resulting in relatively low yield. Stepwise seeded growth of polymer lobes in dispersion polymerization was also developed for colloidal clusters, ^{49,50} which is limited in relatively large particles. For the high-yield synthesis of tetrahedral clusters, various experimental schemes have been proposed and demonstrated. 51-55 Of special note is the random parking scheme of Schade et al., in which four identically charged particles are attached to an oppositely charged core particle producing loosely packed tetrahedral clusters when the core particle size is appropriately chosen. 52 When the size ratio $\alpha = R_{\rm shell}/R_{\rm core}$ is near 2.41, the yield of tetramers is nearly 100% for hard spheres. Gong et al. reported that hybrid compact tetrahedral

Received: May 18, 2021 Published: August 15, 2021





clusters can be prepared by assembling oppositely charged particles onto liquid cores of 3-(trimethoxysilyl) propyl methacrylate (TPM),⁵³ in which particles are partially wetted once they are bound together. Since this colloidal aggregation is limited by balancing repulsive and attractive electrostatic forces, we call it "self-limited ionic self-assembly",^{56,57} which is a high-yield single-step process.

Furthermore, hybrid spherical patchy particles were produced by plasticizing the shell particles that surround liquid cores of silane, causing them to fuse and extrude from the liquid core, which is referred to as "colloidal fusion". During the colloidal fusion process, hidden cores are exposed, forming an intermediate morphology between spherical patchy particles and colloidal clusters, which we call "patchy colloidal particles". He et al. functionalized the cores of hybrid patchy colloidal clusters with DNA which are directly assembled into diamond lattices through a DNA interaction between cores.⁵⁸ Notably, Duguet and his colleagues reported a colloidal chemistry route to uniform hybrid clusters in which polystyrene lobes were grown around vinyl-functionalized silica nanoparticles⁵¹ and patchy colloidal clusters or multidimple particles by additional growth of silica cores,⁵⁹ which was further extended to plasmonic nanoclusters.⁶⁰

Here, we make patchy colloidal clusters of all polymer particles by assembling oppositely charged cross-linked PS particles (shell particles) onto a swollen non-cross-linked plasticized PS particle (core particle). The shell particles approach a core particle due to the long-range electrostatic attraction and then strongly attach and pack at the interface due to the strong wetting force. Then, by a deswelling process, the liquid cores are solidified, producing mechanically stable all-polymer compact colloidal clusters, which can be ideal sacrificial building blocks for inverse diamond or pyrochlore photonic crystals from MgCu₂ structures. 40 Depending on the size ratio, the number of shell particles can be varied as demonstrated in previous reports. 52,53 In addition, by adjusting the swelling ratio of the core particles in the colloidal clusters, the shell particles can be further compressed such that the polymer cores are completely ejected from the centers, which leads to patchy colloidal clusters. Those all-polymer patchy colloidal clusters may be directly assembled into a diamond lattice through the DNA-mediated assembly and turned into inverse diamond photonic crystals after backfilling interstices with inorganic materials.⁵⁸ Alternatively, asymmetric patchy colloidal clusters can be prepared by using silica-PS coreshell particles as the cores and cross-linked PS particles for the shell, in which case the silica nanoparticle is partially ejected from the center during the deswelling process. Finally, we demonstrated that the same asymmetrical structures can be produced with titania-cored PS particles instead of silica-cored ones.

2. RESULTS AND DISCUSSION

2.1. Symmetric Colloidal Clusters by Self-Limited Ionic Self-Assembly. The core PS particles were plasticized and swollen by simple addition of tetrahydrofuran (THF), and shell particles were added in excess at a number ratio of 25:1 to the liquified cores (Figures 1a and S1). The shell particles, which are cross-linked, do not swell significantly. After coordination, the liquid cores with PS shell particles were deswollen by the addition of water to the suspension. Care should be taken to ensure that prior to mixing the shell particles are well-dispersed without any aggregates.

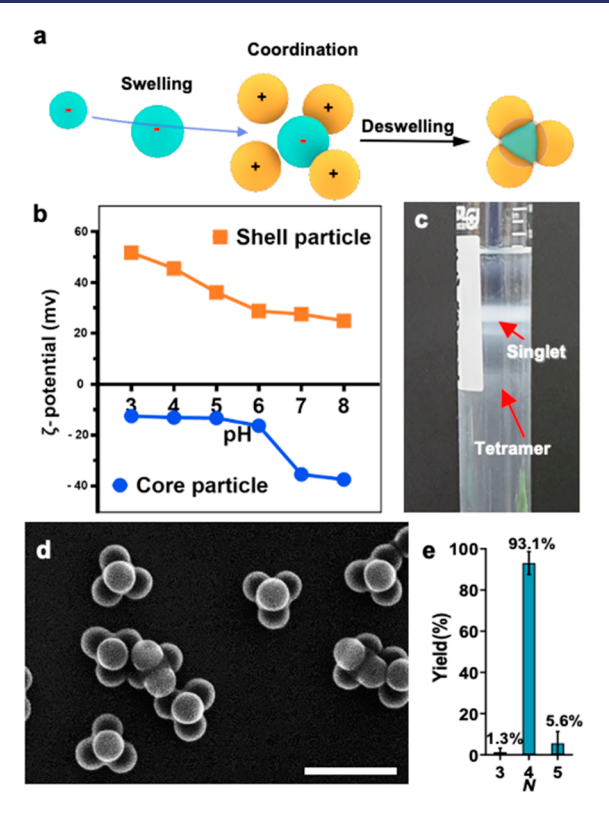


Figure 1. (a) The formation of colloidal clusters by assembling oppositely charged particles. (b) Zeta potential values of core and shell particles at different pH levels. (c) Separation of tetrahedral clusters by density gradient centrifugation. (d) SEM image of tetrahedral clusters. The scale bar is 1 μ m. (e) Statistical distributions of the number of shell particles in cluster N at size ratio $\alpha=1.29$.

We used 332 nm positively charged cross-linked particles as shell particles. At pH 3–5, the zeta potential values were more than 30 mV (Figure 1b) and particles were stable, as shown in optical micrographs of Figure S2. By contrast, particles at pH 6–8 were unstable. For quantitative analysis of colloidal stability, we measured the apparent diameter of particles using inline holographic light scattering (xSight, Spheryx Co.) which can detect only particles larger than 500 nm. ⁶² Thus, we obtained a signal only if aggregates are present. Figure S3, which shows the size and refractive index distribution of measured particles, confirms that shell particles are stable at lower pH. For self-limited ionic self-assembly, ^{56,57} oppositely charged particles were mixed at pH 5.

The core particles were 258 nm negatively charged non-cross-linked PS particles dispersed in a mixture of water and THF with a 3:1 volume ratio (50 mL). Core particles were incubated in a THF—water mixture for 1 h. Then, the 332 nm positively charged cross-linked particles were added to the dispersion of swollen core particles. For the self-limited ionic self-assembly and coordination, the mixture was stirred for 3 h at a speed of 300 rpm. Finally, we added 75 mL of surfactant solution containing Pluronic F108 (1% w/v) into the cluster solution for deswelling the core particles. For complete removal of THF from the cluster solution by evaporation, the cluster solution was thermally annealed at 70 °C for 24 h.

After the formation of colloidal clusters, we separated them from the excess single PS particles (singlets) by density gradient centrifugation. As shown in Figure 1c, one thick band and one thin band are formed in the centrifuge tube.

These correspond to singlets and tetrahedral clusters, respectively (Figures 1d and S4). By analyzing more than 200 clusters in an SEM image, we plotted a histogram in Figure 1e of the yield for a size ratio of $\alpha=1.29$ before swelling. This size ratio for tetrahedral colloidal clusters is a much smaller value than the theoretical value ($\alpha=2.41$) for hard spheres⁵² and for a previous study ($\alpha=1.98$) for liquid-core colloidal clusters. Unlike previous work, no additional salt was added into the system except for HCl for adjusting pH. Therefore, assuming that the salt concentration is $\sim 10~\mu$ M, the Debye screening length is estimated as $\sim 100~\text{nm}^{63,64}$ and the effective size ratio of the swollen core ($\sim 283~\text{nm}$) and charged shell particles (532 nm) becomes 1.87, which is close to the previous experimental data.⁵³

2.2. Symmetric Patchy Colloidal Clusters by Self-Limited Ionic Self-Assembly. By controlling the THF concentration at the swelling step, the morphology of the clusters can be varied, as shown in the schematic diagram of Figure 2. As the concentration of THF increases from 25 to

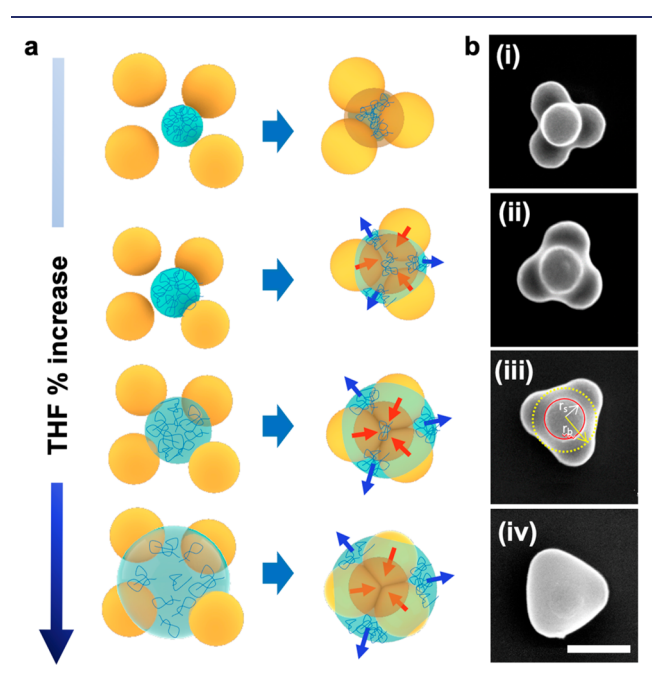


Figure 2. (a) Schematic diagram and (b) SEM images of colloidal clusters of cross-linked polystyrene particles assembled around polystyrene cores swollen with a THF concentration of (i) 25, (ii) 30, (iii) 35, and (iv) 40% v/v in water. The scale bar is 500 nm.

40% v/v in water, the core particles can be swollen more, as shown in Figure S5, so that polystyrene chains are deposited more at outer interstices of shell particles during the deswelling process, leading to patchy particles.

At the lowest THF concentration (25% v/v), the core particles were plasticized and deformed near central interstices between shell particles. As the THF concentration increased, swollen core particles were liquefied completely and became larger than the interstitial space, as shown in the schematic diagram of Figure 2a. However, at higher THF concentration, cross-linked shell PS particles are likely slightly swollen in the swelling step (Figure S6), enough that the inside surface of shell particles can be deformed under the compressive capillary force in the final cluster packing stage during the deswelling process. Indeed, as the THF concentration is increased, the central space of the clusters is filled with deformed shell

particles and polymers in the liquefied cores are ejected and fill the outer surface between shell particles (Figure 2b). Notably, all of the clusters have the same diameter of the circumscribed circle.

As shown in the SEM images, colloidal clusters evolved into patchy colloidal clusters as the core particles are increasingly swollen with THF. Their morphologies can be characterized with the size ratio of the body to shell particles ($\lambda = r_b/r_s$), as shown in Figure 2b (iii), which is a key geometric parameter for the successful assembly of colloidal diamond and pyrochlore lattices. For patchy colloidal clusters in Figure 2b, the λ values were 1.16, 1.39, 1.5, and 1.71 for (i), (ii), (iii), and (iv), respectively. In the case of 40% THF in water (iv), cross-linked shell particles in clusters are completely covered with polystyrene, which might be interesting in the packings of truncated tetrahedra for another type of diamond lattice. In these patchy particles, lobes and matrix may be functionalized with different surface charges or DNA, shich leads to the direct formation of open colloidal superstructures.

2.3. Symmetric Hybrid Patchy Colloidal Clusters of Silica and PS Particles. To increase the density mismatch between clusters and singlets, we have prepared silica—PS core—shell particles for the core (Figure 3a) instead of pure

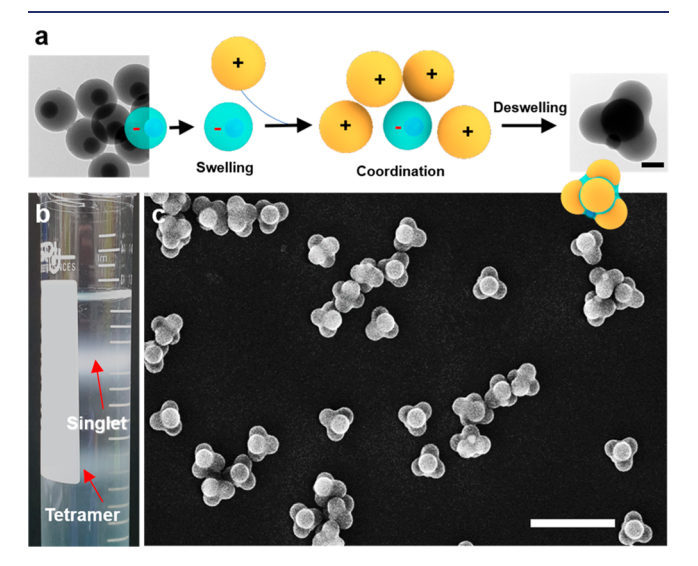


Figure 3. (a) Hybrid clusters using silica—PS core—shell particles as cores. Inset TEM images show core—shell particles on the left and silica nanoparticles at the surface between PS clusters on the right. (b) Density gradient medium with two bands of polystyrene particles on the top and tetrahedral clusters with silica nanoparticles in the bottom. (c) SEM image of colloidal clusters with silica cores. Scale bars are 200 nm in the inset of part a and 2 μ m in part c.

polymer particles, which should improve the separation efficiency for density gradient centrifugation. The silica particles were synthesized by the Stöber method, producing particles with an average diameter of 170 nm. Then, as shown in the inset TEM image on the left of Figure 3a and the SEM image of Figure S7a, polystyrene shell layers were grown by emulsion polymerization on vinyl-silane modified silica particles. The silica particles are not positioned at the center as reported in a previous article. The final diameter of the core—shell particles was 384 nm on average. For the shell particle, we used a 431 nm PS particle with $\alpha = 1.12$.

As illustrated in Figure 3a, first we dispersed the core particles in THF solution (25% v/v in water), which was aged

for 1 h for swelling the polystyrene shell. For the following coordination step, the pH of the solution was set to 5, in which both are highly charged in solution (Figure S8). Then, positively charged cross-linked polystyrene particles were added into the dispersion of swollen core-shell particles and gently stirred for 3 h. Finally, we added 75 mL of surfactant solution containing Pluronic F108 (1% w/v) into the cluster solution for deswelling the core particles, which produced colloidal clusters of polystyrene and silica, as shown in the inset TEM image on the right of Figure 3a. Due to the relocation of silica nanoparticles in the core, the tetrahedral symmetry is broken, which may be useful for assembling less symmetric or more complex structures. For cluster separation from singlets, the density gradient centrifugation was performed. Because the ratio of silica to PS is different in singlets and clusters, their densities are different, which improves the separation, as indicated by the distinct bands in the density gradient centrifuge tube (Figure 3b). As shown in Figures 3c and S9, tetrahedral clusters of polystyrene particles with silica nanoparticles were successfully obtained.

The number of shell particles N in the clusters can be controlled by changing the size ratio α of the shell to the core. To this end, in addition to 431 nm ($\alpha=1.12$), we prepared 422 and 494 nm positively charged PS particles for shells (Figure S7b-d), which corresponds to $\alpha=1.10$ and 1.29, respectively. The resulting clusters in Figure 4a-c were pentamers, tetramers, and trimers for $\alpha=1.10$, 1.12, and 1.29, respectively. By analyzing more than 200 clusters in SEM images, we plotted the histograms of yield in Figure 4d-f, which were higher than 85% for all cases.

For fixed α , the distribution of constituent particles N in clusters can also be controlled by adjusting the solution pH. When the pH is lower, the surface charge density of the shell particles is higher (Figure S10). Therefore, the effective size of the shell particles increased, which resulted in lower α or N. As shown in Figure S10, for $\alpha = 1.12$, trimers and tetramers are obtained in a nearly 80% yield, when pH 3 and 4, respectively. For pH 5, the yield of tetramers was more than 90%, which suggested that the effective size ratio was closer to the ideal value.

2.4. Asymmetric Hybrid Patchy Colloidal Clusters of Silica and PS Particles. When the size ratio of silica nanoparticles to shell PS particles (β) is small enough, the symmetry of the shell particles can be kept, as demonstrated in the previous section. By contrast, when silica particles become larger, the symmetry of clusters can be broken. As shown in Figures S11 and 5d, 288 nm core—shell particles with 95 nm silica particles (β = 0.32) and 296 nm shell particles were prepared and assembled into clusters, as shown in Figure 5a, in which small silica cores were still embedded inside polymers. For core—shell particles with β = 0.39 (Figure 5e), small silica cores are clearly observed for N = 3–5 in all SEM images in Figure 5b but shell particles keep their symmetric configurations.

For a higher size ratio of β = 0.66 (Figure 5f), 504 nm coreshell particles with 338 nm silica cores were prepared and assembled with 511 nm positively charged cross-linked PS particles (Figure S12). We observed the silica cores for all clusters (N = 2-5), as shown in the SEM images of Figure 5c, and they keep the symmetric configuration of shell particles for N = 2 and 3. However, for N = 4 and 5, symmetries of shell particles were broken due to the large silica nanoparticles. These asymmetric configurations of colloidal clusters are

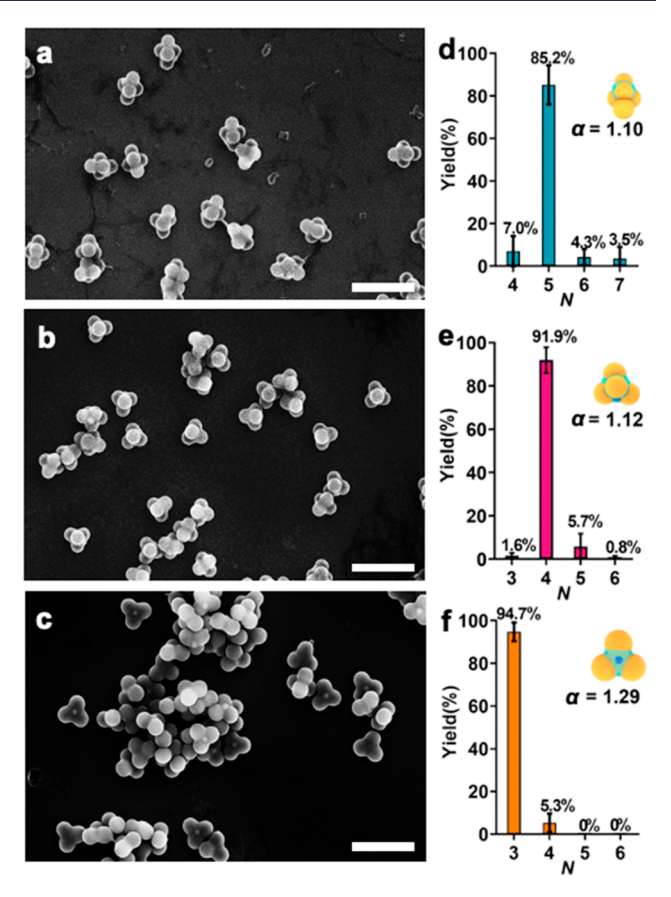


Figure 4. (a–c) SEM images of clusters and (d–f) distributions of the number of shell particles in cluster N when (a, d) α = 1.10, (b, e) α = 1.12, and (c, f) α = 1.29. (d–f) Statistical distributions of the number of shell particles in cluster N for clusters that form at various size ratios α ; size ratios α are shown in the graph, and every scale bar is 2 μ m. The vertical lines are error bars representing standard deviation.

consistent for N=4 and 5. In our hybrid clusters, lobes can be functionalized with different charges or DNA, which may lead to open three-dimensional or two-dimensional colloidal superstructures, as predicted in computer simulation. Furthermore, asymmetric clusters can serve as building blocks of chiral superstructures which would be potentially useful in chiral metamaterials or topological photonic insulators. $^{67-70}$

The origin of the asymmetric configuration can be better understood from a "Surface Evolver" (developed by K. Brakke) simulation, as shown in Figure 6.^{71,72} As the volume of the core swollen particle is reduced gradually, the surface energies decrease. The code, which we used for cluster formation in evaporating droplets, was developed by Lauga et al.⁷³ Initially, the volume of the core was set as 1 and PS-shell particles (yellow spheres) were set as 0.0156. The four PS-shell particles and one silica particle (blue sphere) on the core (cyan sphere) were rearranged and reformed into compact clusters when the core volume was reduced gradually until the same as 0.007. In this simulation, the contact angle between the core and the PS-shell was set at 20° and that between the core surface and the silica particle was set at 5° . When the size ratio of silica nanoparticles to shell PS particles (β) is less than 0.6, polystyrene shell particles keep their tetrahedral symmetry, as shown in Figure 6a–c. However, for $\beta \ge 0.6$, the symmetry of polystyrene shell particles can be broken, as shown in Figure 6d-f. As expected, depending on the wetting angle between

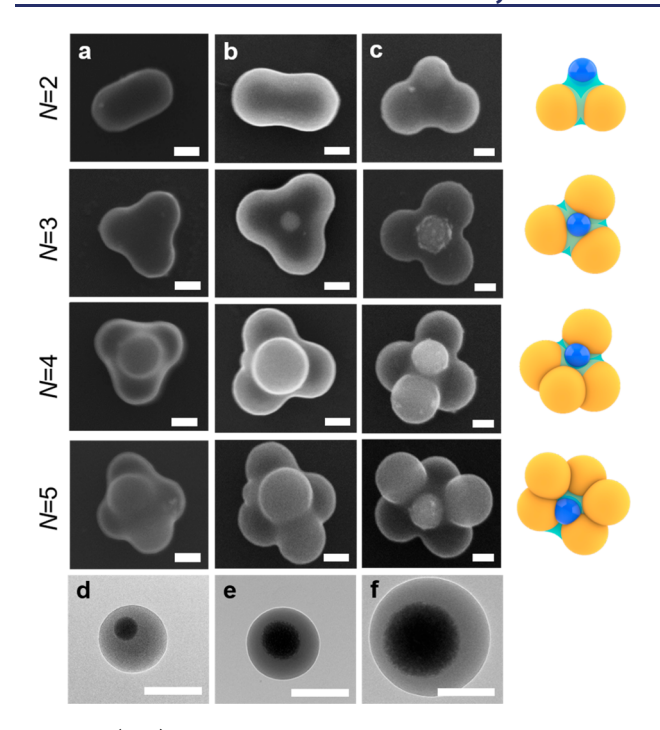


Figure 5. (a–c) SEM images of hybrid clusters for N=2-5 using silica–PS core–shell particles as cores in (d–f) TEM images. Every scale bar is 200 nm. The diameter of silica particles is (a) 95 nm, (b) 170 nm, and (c) 338 nm, and the diameter of silica–PS core–shell particle is (a) 288 nm, (b) 384 nm, and (c) 504 nm. Every scale bar is 200 nm.

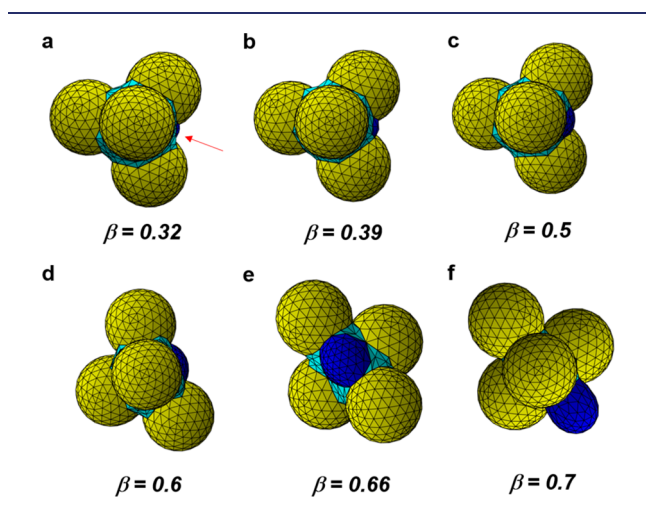


Figure 6. Configurations of polystyrene shell particles and silica nanoparticles around polystyrene spheres for size ratios of silica nanoparticles to shell PS particles (β) of (a) 0.32 (b) 0.39 (c) 0.5, (d) 0.6, (e) 0.66, and (f) 0.7, which were predicted by Surface Evolver simulation. The volume ratio of silica—PS core—shell particles to shell particles is 0.449.

the silica sphere and the liquid core, the critical value of β for symmetry breaking can be changed, as shown in Figure 6.

2.5. Asymmetric Hybrid Patchy Colloidal Clusters of Titania and PS Particles. Instead of silica—polystyrene core—shell particles, we have utilized titania—polystyrene core—shell particles, which showed the same configurations of polystyrene shell particles, as shown in Figure 7. For anatase titania particles on titania—PS core—shell particles, amorphous titania particles with ~500 nm in diameter were prepared by

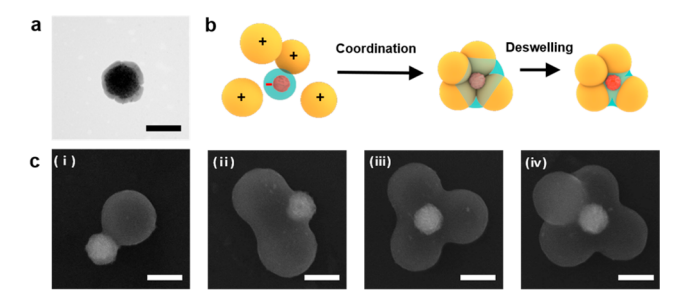


Figure 7. (a) TEM image of anatase titania—PS core—shell particles. (b) The schematic diagram of cluster formation of cross-linked PS particles with titania—PS core—shell nanoparticles. (c) SEM images of titania—PS hybrid clusters of which the number of cross-linked PS particles (N) is (i) 1, (ii) 2, (iii) 3, and (iv) 4. Every scale bar is 500 nm.

sol-gel reaction and thermally annealed at 500 $^{\circ}$ C in which particles were shrunken down to \sim 400 nm, as shown in Figure S13b.

Anatase titania particles were modified with vinyl silane and PS shell layers were grown by emulsion polymerization, as shown in the electron micrographs of Figure 7a and Figure S13b,c. 66 Then, colloidal clusters were prepared as illustrated in Figure 7b. At first, we dispersed the core particles in THF solution (25% v/v in water), which was incubated for 1 h for swelling the PS shell. In the coordination step, the pH of the solution was set to 5 by adjusting the concentration of HCl. Then, 765 nm diameter positively charged cross-linked PS particles (Figure S13a) were added into the dispersion of swollen core—shell particles and gently stirred for 3 h. Finally, we added 75 mL of surfactant solution containing Pluronic F108 (1% w/v) into the cluster solution for deswelling the core particles, which produced colloidal clusters of PS and titania, as shown in the inset SEM images in Figures 7c and S14.

The same configurations of clusters, which we have with the silica nanoparticles in Figure 5, were observed in hybrid clusters with titania particles. The size ratio β of titania nanoparticles to shell PS particles was 0.52. However, the configuration for four PS shell particles is not consistent with our prediction in Figure 6c. The discrepancy may come from the different volume ratio of the PS core to the shell particle (γ) . In other words, the polystyrene shell on the titania core particle is much thinner than that on silica, as shown in Figure 7a. In the Surface Evolver simulation, the configuration of the cluster with the titania particle was matched, as shown in Figure S15 when the contact angle between the PS core and PS shell particles and core and titania particles is 50 and 30°, respectively. These results imply that we can generalize our method for asymmetric clusters. Since titania is an efficient photocatalytic material, those asymmetric hybrid clusters can be further utilized as colloidal swimmers under UV irradiation for investigating non-equilibrium colloidal structures. 74,75

3. CONCLUSIONS

We have presented a way of synthesizing polymer-cored colloidal clusters by self-limited ionic self-assembly. Positively charged PS particles were closely packed around negatively charged swollen PS particles. Then, by plasticizing the cores, polymer-cored colloidal clusters were produced. When the size ratio of shell to core particles was optimized, high-purity symmetric tetrahedral colloidal clusters were obtained. Our all-polymer colloidal clusters can be ideal sacrificial building

blocks for inverse diamond or pyrochlore photonic crystals. As the swelling ratio of the core increased, colloidal clusters evolved to cored clusters and patchy particles. Furthermore, by utilizing silica—PS core—shell particles as the core, asymmetric hybrid colloidal clusters were produced in which each silica core was relocated to the interface during the swelling—deswelling process. Since hybrid clusters are heavier than PS particles, they can be easily purified by density gradient centrifugation and further by isopycnic centrifugation if necessary. Uniform asymmetric colloidal clusters could be key building blocks for chiral photonic structures^{67–70} and direct assembly of diamond photonic structures^{76,77} or self-propelling swimmers for non-equilibrium superstructures.^{74,78}

4. MATERIALS AND METHODS

- 4.1. Materials. Styrene (previously purified with inhibitor remover, ≥99%), poly(ethylene glycol)-block-poly(propylene glycol)-block-poly(ethylene glycol) (F108, $M_w \sim 14,600$), sodium dodecyl sulfate (SDS, ACS reagent, ≥99%), 3-(trimethoxysilyl)propyl methacrylate (TPM, ≥97%), divinylbenzene (previously purified with inhibitor remover, DVB, technical grade, 80%), sodium bicarbonate (\geq 99.7%), sodium hydroxide (\geq 98%), tetraethyl orthosilicate (TEOS, ≥99.0%), dodecylamine (98%), titanium(iv) isopropoxide (TTIP, 97%), acetonitrile (anhydrous, 99.8%), and methanol (anhydrous, 99.8%) were purchased from Sigma-Aldrich. Potassium persulfate (KPS, 98.0%), tetrahydrofuran (THF, 99.5%), anhydrous ethanol (99.9%), hydrochloric acid solution (HCl, 0.1 M), deionized water (DI water), and ammonia solution (28.0-30.0%) were purchased from Samchun Pure Chemical Co. Sodium chloride (NaCl, 99%) was purchased from Junsei. 2,2'-Azobis(2-methylpropionamidine) dihydrochloride (AIBA, 98%) was purchased from
- **4.2.** Synthesis of Negatively Charged Non-Cross-Linked Polystyrene (PS) Particles for Core Particles. PS particles were synthesized using surfactant-free emulsion polymerization. Polymerization of negatively charged non-cross-linked PS particles, 258 nm in diameter, was carried out under a nitrogen atmosphere. Styrene (7 mL), DI water (50 mL), and NaCl (0.018 g) were added into a 100 mL three-neck round-bottom flask. The reaction temperature was gradually heated to 70 °C with stirring using a magnetic stir bar at a speed of 500 rpm. After 1 h, KPS (0.03 g) dissolved in the DI water (5 mL) was injected into a reactor. The reactor was kept at 70 °C for 24 h. After the polymerization, PS particles were washed and resuspended by sonication in ethanol and water several times. After washing of PS particles, PS particles were resuspended in DI water.
- 4.3. Synthesis of Positively Charged Cross-Linked PS Particles for Shell Particles. Polymerization of positively charged cross-linked PS particles, 332 nm in diameter, was carried out under a nitrogen atmosphere. Styrene (5 mL), DI water (50 mL), and DVB (0.5 mL) were added into a 100 mL three-neck round-bottom flask. The reaction temperature was gradually heated to 70 °C with stirring using a magnetic stir bar at a speed of 500 rpm. After 1 h, AIBA (0.07 g) dissolved in the DI water (1 mL) was injected into a reactor. The reactor was kept at 70 °C for 24 h. After the polymerization, PS particles were washed and resuspended by sonication in ethanol and water several times. After the washing of PS particles, PS particles were resuspended in DI water. For polymerization of 296, 422, 431, 494, 511, and 785 nm diameter of positively charged cross-linked PS particles, styrene (4.5, 8, 9, 12, 13, and 20 mL), DI water (100 mL), DVB (0.45, 0.8, 0.9, 1.2, 1.3, and 2 mL), and AIBA (0.14 g) dissolved in DI water (1 mL) were used. All procedures are the same as polymerization of positively charged cross-linked PS particles, 332 nm
- **4.4. Synthesis of Silica-PS Core-Shell Particles.** For silica particles on silica-PS particles, silica with 170 nm diameter was prepared by the Stöber method at ambient temperature. ⁶⁶ TPM (5 mL) in ethanol was dropped into the dispersion of silica particles for 8 h with stirring using a magnetic stirrer at a speed of 800 rpm. After 40

h, silica particles were obtained and washed several times using ethanol. After drying out the silica particles, 1.2 g of silica particles was dispersed in 10 mL of ethanol. Synthesis of silica—PS was carried out under the nitrogen atmosphere in a 100 mL three-neck round-bottom flask. SDS (0.03 g) and sodium bicarbonate (0.24 g) were put into a reactor with 100 mL of DI water. The reactor's temperature was gradually increased at 80 °C. Then, styrene (10 mL) was injected into the reactor. After 30 min, KPS (0.1 g) dissolved into 5 mL of DI water was injected into the reactor. The synthesis of 384 nm diameter silica—PS particles was finished after 24 h. Silica—PS particles were washed several times with ethanol and DI water and kept resuspended in DI water.

- 4.5. Synthesis of Anatase Titania-PS Core-Shell Particles. For anatase titania particles on titania-PS core-shell particles, titania particles with 500 nm diameter were prepared by a hydrolysis and condensation reaction.⁷⁸ Synthesized titania particles were washed with ethanol and water and dried. Titania powder was calcined and transformed to the anatase phase, which was described in previous results.⁷⁹ Anatase titania powder was dispersed in ethanol, and the TPM (5 mL) in the ethanol was dropped into the dispersion of anatase titania particles for 8 h with stirring using a magnetic stirrer at a speed of 800 rpm. 80 After 40 h, titania particles were obtained and washed several times using ethanol. After drying out the titania particles in a vacuum state, 0.1 g of anatase titania particles was dispersed in 1 mL of ethanol. Synthesis of titania-PS core-shell particles was carried out under a nitrogen atmosphere in a 50 mL three-neck round-bottom flask. SDS (0.01 g) and sodium bicarbonate (0.15 g) were put into a reactor with 20 mL of DI water. The reactor's temperature was gradually increased at 80 °C. Then, styrene (3 mL) was injected into the reactor. After 30 min, KPS (0.03 g) dissolved into 1 mL of DI water was injected into the reactor. The synthesis of anatase titania-PS particles was finished after 24 h. Titania-PS particles were washed several times with ethanol and DI water and kept resuspended in DI water.
- **4.6. Formation of a Cluster.** Twenty μ L suspensions of core particles (2% w/v) were added in 50 mL of THF solution (25% v/v). When we made the THF solution, we used an acidic water solution which is the mixture of HCl and water. After swelling the core particles for 1 h, 200 μ L suspensions of shell particles (5% w/v) were added in the THF solution. We set a shell-to-core ratio of 25:1. To allow enough time for the core particles to coordinate with the shell particles, the core and shell particle solutions were stirred for 3 h at a speed of 300 rpm. After the coordination time, we poured 75 mL of 1% w/v F108 solution in water into the stirred cluster solution to deswell the core particles. To be sure to evaporate THF completely from the cluster solution, we annealed it at 70 °C for 24 h.
- **4.7. Density Gradient Centrifugation.** To make a 5-22% v/v linear gradient of glycerol in water solution, a gradient mixer (size 30 mL, Sigma-Aldrich) was used. ¹⁹ We prepared a glycerol solution in 1% w/v F108/water solution. Cluster suspension (0.5 mL) was loaded on top of the gradient solution. The setting of the centrifugation was for 1 h at $2800 \times g$, and the sample was centrifuged with a swinging bucket rotor. Then, we extracted clusters using the syringe with a long stainless needle. The extracted clusters were washed several times with ethanol and DI water.
- **4.8. Characterizations.** Colloidal particles in the solution were imaged by optical microscope (Nikon, Eclipse Ti-U). Colloidal particles in the dried state were imaged by scanning electron microscopy (SEM, Hitachi, Hitachi S-4300 and S-4800) and transmission electron microscopy (TEM, JEOL LTD, JEM-2100F, JEM-2200FS, and JEM-3010). Swollen colloidal particles were imaged by environmental scanning electron microscopy (ESEM, Thermo-Fisher Scientific, Quattro S). Elemental compositions were determined by energy dispersive spectroscopy (EDS) using TEM. SEM samples were prepared by depositing the washed sample on a silicon wafer, and platinum sputtering coating was applied on the deposited sample. TEM samples were prepared by depositing the washed sample on a carbon film (Electron Microscopy Science, CF200-Cu) and a holey carbon film (Electron Microscopy Science, HC300-CU). Zeta potential values of colloidal particles were

measured by a Zetasizer (Malvern Panalytical, Zetasizer Nano S). The data for holographic particle characterization was measured by xSight (Spheryx Inc., xSight). All pH values of the solutions were evaluated by a pH meter (Mettler-Toledo Instruments, FiveEasy Plus pH meter).

ASSOCIATED CONTENT

Supporting Information

The Supporting Information is available free of charge at https://pubs.acs.org/doi/10.1021/jacs.1c05123.

SEM, TEM, ESEM, and optical microscopy images, EDS mapping data of hybrid clusters, holographic characterization of particles, zeta-potential, and Surface Evolver simulation (PDF)

AUTHOR INFORMATION

Corresponding Author

Gi-Ra Yi — School of Chemical Engineering, Sungkyunkwan University, Suwon, Gyeonggi 16419, Republic of Korea; Department of Chemical Engineering, POSTECH, Pohang, Gyeongbuk 37673, Republic of Korea; orcid.org/0000-0003-1353-8988; Email: yigira@postech.ac.kr

Authors

You-Jin Kim — School of Chemical Engineering, Sungkyunkwan University, Suwon, Gyeonggi 16419, Republic of Korea; Occid.org/0000-0001-7168-7856

Jae-Hyun Kim — School of Chemical Engineering, Sungkyunkwan University, Suwon, Gyeonggi 16419, Republic of Korea

In-Seong Jo – School of Chemical Engineering, Sungkyunkwan University, Suwon, Gyeonggi 16419, Republic of Korea

David J. Pine — Department of Physics, New York University, New York, New York 10003, United States; Department of Chemical & Biomolecular Engineering, New York University, Brooklyn, New York 11201, United States; orcid.org/0000-0002-3304-6684

Stefano Sacanna — Department of Chemistry, New York University, New York, New York 10003, United States; orcid.org/0000-0002-8399-3524

Complete contact information is available at: https://pubs.acs.org/10.1021/jacs.1c05123

Author Contributions

 ${}^{
abla}\! ext{Y.-J.K., J.-H.K.:}$ These authors contributed equally.

Notes

The authors declare no competing financial interest.

ACKNOWLEDGMENTS

This research has been supported by the National Research Foundation of Korea (NRF) (2017M3A7B8065528, 2021R1A2C3013800). D.J.P. was supported by the US Army Research Office under grant award number W911NF-17-1-0328. S.S. was supported by the NSF CAREER award DMR-1653465.

REFERENCES

- (1) Pieranski, P. Colloidal crystals. Contemp. Phys. 1983, 24 (1), 25–73.
- (2) Kalsin, A. M.; Fialkowski, M.; Paszewski, M.; Smoukov, S. K.; Bishop, K. J. M.; Grzybowski, B. A. Electrostatic self-assembly of binary nanoparticle crystals with a diamond-like lattice. *Science* **2006**, 312 (5772), 420–424.

- (3) Shevchenko, E. V.; Talapin, D. V.; Kotov, N. A.; O'Brien, S.; Murray, C. B. Structural diversity in binary nanoparticle superlattices. *Nature* **2006**, 439 (7072), 55–59.
- (4) Zhuang, J.; Wu, H.; Yang, Y.; Cao, Y. C. Supercrystalline colloidal particles from artificial atoms. *J. Am. Chem. Soc.* **2007**, *129* (46), 14166–14167.
- (5) Alsayed, A. M.; Islam, M. F.; Zhang, J.; Collings, P. J.; Yodh, A. G. Premelting at defects within bulk colloidal crystals. *Science* **2005**, 309 (5738), 1207–1210.
- (6) Aryana, K.; Stahley, J. B.; Parvez, N.; Kim, K.; Zanjani, M. B. Superstructures of multielement colloidal molecules: Efficient pathways to construct reconfigurable photonic and phononic crystals. *Adv. Theory Simul.* **2019**, 2 (5), 1800198.
- (7) Hueckel, T.; Hocky, G. M.; Palacci, J.; Sacanna, S. Ionic solids from common colloids. *Nature* **2020**, *580* (7804), 487–490.
- (8) Manoharan, V. N. Colloidal matter: Packing, geometry, and entropy. Science 2015, 349 (6251), 1253751.
- (9) Liu, Z.; Zhang, X.; Mao, Y.; Zhu, Y. Y.; Yang, Z.; Chan, C. T.; Sheng, P. Locally resonant sonic materials. *Science* **2000**, 289 (5485), 1734–1736.
- (10) Maldovan, M. Sound and heat revolutions in phononics. *Nature* **2013**, 503 (7475), 209–217.
- (11) Graczykowski, B.; Vogel, N.; Bley, K.; Butt, H.-J.; Fytas, G. Multiband hypersound filtering in two-dimensional colloidal crystals: Adhesion, resonances, and periodicity. *Nano Lett.* **2020**, *20* (3), 1883–1889.
- (12) Perro, A.; Reculusa, S.; Ravaine, S.; Bourgeat-Lami, E.; Duguet, E. Design and synthesis of janus micro- and nanoparticles. *J. Mater. Chem.* **2005**, *15* (35–36), 3745–3760.
- (13) Decuzzi, P.; Ferrari, M. The receptor-mediated endocytosis of nonspherical particles. *Biophys. J.* **2008**, *94* (10), 3790–3797.
- (14) Yang, S.-M.; Kim, S.-H.; Lim, J.-M.; Yi, G.-R. Synthesis and assembly of structured colloidal particles. *J. Mater. Chem.* **2008**, *18* (19), 2177–2190.
- (15) Mitragotri, S.; Lahann, J. Physical approaches to biomaterial design. *Nat. Mater.* **2009**, *8* (1), 15–23.
- (16) Lee, K. J.; Yoon, J.; Lahann, J. Recent advances with anisotropic particles. *Curr. Opin. Colloid Interface Sci.* **2011**, *16* (3), 195–202.
- (17) Sacanna, S.; Pine, D. J. Shape-anisotropic colloids: Building blocks for complex assemblies. *Curr. Opin. Colloid Interface Sci.* **2011**, 16 (2), 96–105.
- (18) Ben Zion, M. Y.; He, X.; Maass, C. C.; Sha, R.; Seeman, N. C.; Chaikin, P. M. Self-assembled three-dimensional chiral colloidal architecture. *Science* **2017**, 358 (6363), 633–636.
- (19) Manoharan, V. N.; Elsesser, M. T.; Pine, D. J. Dense packing and symmetry in small clusters of microspheres. *Science* **2003**, *301* (5632), 483–487.
- (20) Ngo, T. T.; Liddell, C. M.; Ghebrebrhan, M.; Joannopoulos, J. D. Tetrastack: Colloidal diamond-inspired structure with omnidirectional photonic band gap for low refractive index contrast. *Appl. Phys. Lett.* **2006**, *88* (24), 241920.
- (21) Hynninen, A.-P.; Thijssen, J. H. J.; Vermolen, E. C. M.; Dijkstra, M.; van Blaaderen, A. Self-assembly route for photonic crystals with a bandgap in the visible region. *Nat. Mater.* **2007**, *6* (3), 202–205
- (22) Forster, J. D.; Park, J.-G.; Mittal, M.; Noh, H.; Schreck, C. F.; O'Hern, C. S.; Cao, H.; Furst, E. M.; Dufresne, E. R. Assembly of optical-scale dumbbells into dense photonic crystals. *ACS Nano* **2011**, *5* (8), 6695–6700.
- (23) Morozov, K. I.; Leshansky, A. M. Photonics of template-mediated lattices of colloidal clusters. *Langmuir* **2019**, 35 (11), 3987–3991
- (24) Avvisati, G.; Dasgupta, T.; Dijkstra, M. Fabrication of colloidal laves phases via hard tetramers and hard spheres: Bulk phase diagram and sedimentation behavior. *ACS Nano* **2017**, *11* (8), 7702–7709.
- (25) Wang, Y.; Wang, Y.; Breed, D. R.; Manoharan, V. N.; Feng, L.; Hollingsworth, A. D.; Weck, M.; Pine, D. J. Colloids with valence and specific directional bonding. *Nature* **2012**, *491* (7422), 51–55.

- (26) Zhang, Z.; Glotzer, S. C. Self-assembly of patchy particles. *Nano Lett.* **2004**, *4* (8), 1407–1413.
- (27) Zanjani, M. B.; Jenkins, I. C.; Crocker, J. C.; Sinno, T. Colloidal cluster assembly into ordered superstructures via engineered directional binding. ACS Nano 2016, 10 (12), 11280–11289.
- (28) Zanjani, M. B.; Crocker, J. C.; Sinno, T. Self-assembly with colloidal clusters: facile crystal design using connectivity landscape analysis. *Soft Matter* **2017**, *13*, 7098–7105.
- (29) Ma, Y.; Ferguson, A. L. Inverse design of self-assembling colloidal crystals with omnidirectional photonic bandgaps. *Soft Matter* **2019**, *15*, 8808–8826.
- (30) Aryana, K.; Stahley, J. B.; Parvez, N.; Kim, K.; Zanjani, M. B. Superstructures of multielement colloidal molecules: Efficient pathways to construct reconfigurable photonic and phononic crystals. *Adv. Theory Simul.* **2019**, *2* (5), 1800198.
- (31) Rocha, B. C.; Paul, S.; Vashisth, H. Enhanced porosity in self-assembled morphologies mediated by charged lobes on patchy particles. *J. Phys. Chem. B* **2021**, *125* (12), 3208–3215.
- (32) Morphew, D.; Shaw, J.; Avins, C.; Chakrabarti, D. Programming hierarchical self-assembly of patchy particles into colloidal crystals via colloidal molecules. *ACS Nano* **2018**, *12* (3), 2355–2364.
- (33) Rao, A. B.; Shaw, J.; Neophytou, A.; Morphew, D.; Sciortino, F.; Johnston, R. L.; Chakrabarti, D. Leveraging hierarchical self-assembly pathways for realizing colloidal photonic crystals. *ACS Nano* **2020**, *14* (5), 5348–5359.
- (34) Neophytou, A.; Manoharan, V. N.; Chakrabarti, D. Self-assembly of patchy colloidal rods into photonic crystals robust to stacking faults. *ACS Nano* **2021**, *15* (2), 2668–2678.
- (35) Wang, Y.; Wang, Y.; Zheng, X.; Ducrot, É.; Yodh, J. S.; Weck, M.; Pine, D. J. Crystallization of DNA-coated colloids. *Nat. Commun.* **2015**, *6* (1), 1–8.
- (36) Moon, J.; Jo, I.-S.; Ducrot, E.; Oh, J. S.; Pine, D. J.; Yi, G.-R. DNA-coated microspheres and their colloidal superstructures. *Macromol. Res.* **2018**, 26 (12), 1085–1094.
- (37) Wang, Y.; Wang, Y.; Zheng, X.; Ducrot, É.; Lee, M.-G.; Yi, G.-R.; Weck, M.; Pine, D. J. Synthetic strategies toward DNA-coated colloids that crystallize. *J. Am. Chem. Soc.* **2015**, *137* (33), 10760–10766
- (38) Oh, J. S.; Wang, Y.; Pine, D. J.; Yi, G.-R. High-density PEO-b-DNA brushes on polymer particles for colloidal superstructures. *Chem. Mater.* **2015**, *27* (24), 8337–8344.
- (39) Oh, J. S.; Lee, S.; Glotzer, S. C.; Yi, G.-R.; Pine, D. J. Colloidal fibers and rings by cooperative assembly. *Nat. Commun.* **2019**, *10* (1), 1–10.
- (40) Ducrot, É.; He, M.; Yi, G.-R.; Pine, D. J. Colloidal alloys with preassembled clusters and spheres. *Nat. Mater.* **2017**, *16* (6), 652–657
- (41) Yablonovitch, E. Inhibited spontaneous emission in solid-state physics and electronics. *Phys. Rev. Lett.* **1987**, *58* (20), 2059.
- (42) Ducrot, É.; Gales, J.; Yi, G.-R.; Pine, D. J. Pyrochlore lattice, self-assembly and photonic band gap optimizations. *Opt. Express* **2018**, 26 (23), 30052–30060.
- (43) Gondaira, K.; Ishizaki, K.; Kitano, K.; Asano, T.; Noda, S. Control of radiation angle by introducing symmetric end structure to oblique waveguide in three-dimensional photonic crystal. *Opt. Express* **2016**, 24 (12), 13518–13526.
- (44) Noda, S.; Tomoda, K.; Yamamoto, N.; Chutinan, A. Full three-dimensional photonic bandgap crystals at near-infrared wavelengths. *Science* **2000**, 289 (5479), 604–606.
- (45) Aoki, K.; Guimard, D.; Nishioka, M.; Nomura, M.; Iwamoto, S.; Arakawa, Y. Coupling of quantum-dot light emission with a three-dimensional photonic-crystal nanocavity. *Nat. Photonics* **2008**, *2* (11), 688–692.
- (46) Pazos-Perez, N.; Wagner, C. S.; Romo-Herrera, J. M.; Liz-Marzán, L. M.; de Abajo, F. J. G.; Wittemann, A.; Fery, A.; Alvarez-Puebla, R. A. Organized Plasmonic Clusters with High Coordination number and extraordinary enhancement in surface-enhanced Raman

- scattering (SERS). Angew. Chem., Int. Ed. 2012, 51 (51), 12688-12693.
- (47) Ku, K. H.; Kim, Y. J.; Yi, G.-R.; Jung, Y. S.; Kim, B. J. Soft Patchy Particles of Block Copolymers from Interface-Engineered Emulsions. ACS Nano 2015, 9 (11), 11333–11341.
- (48) Gröschel, A. H.; Walther, A.; Löbling, T. I.; Schacher, F. H.; Schmalz, H.; Müller, A. H. E. Guided hierarchical co-assembly of soft patchy nanoparticles. *Nature* **2013**, *503*, 247–251.
- (49) Kim, J.-W.; Larsen, R. J.; Weitz, D. A. Uniform Nonspherical Colloidal Particles with Tunable Shapes. *Adv. Mater.* **2007**, *19* (15), 2005–2009.
- (50) Liu, M.; Dong, F.; Jackson, N. S.; Ward, M. D.; Weck, M. Customized chiral colloids. *J. Am. Chem. Soc.* **2020**, *142* (39), 16528–16532.
- (51) Désert, A.; Chaduc, I.; Fouilloux, S.; Taveau, J.-C.; Lambert, O.; Lansalot, M.; Bourgeat-Lami, E.; Thill, A.; Spalla, O.; Ravaine, S.; Duguet, E. High-yield preparation of polystyrene/silica clusters of controlled morphology. *Polym. Chem.* **2012**, *3* (5), 1130–1132.
- (52) Schade, N. B.; Holmes-Cerfon, M. C.; Chen, E. R.; Aronzon, D.; Collins, J. W.; Fan, J. A.; Capasso, F.; Manoharan, V. N. Tetrahedral colloidal clusters from random parking of bidisperse spheres. *Phys. Rev. Lett.* **2013**, *110* (14), 148303.
- (53) Gong, Z.; Hueckel, T.; Yi, G.-R.; Sacanna, S. Patchy particles made by colloidal fusion. *Nature* **2017**, *550* (7675), 234–238.
- (54) McGinley, J. T.; Wang, Y.; Jenkins, I. C.; Sinno, T.; Crocker, J. C. Crystal-templated colloidal clusters exhibit directional DNA interactions. ACS Nano 2015, 9 (11), 10817–10825.
- (55) Yuan, Q.; Gu, J.; Zhao, Y.; Yao, L.; Guan, Y.; Zhang, Y. Synthesis of a colloidal molecule from soft microgel spheres. ACS Macro Lett. 2016, 5 (5), 565–568.
- (56) Hou, K.; Han, J.; Tang, Z. Formation of Supraparticles and Their Application in Catalysis. *ACS Materials Lett.* **2020**, 2 (1), 95–106.
- (57) Xia, Y.; Nguyen, T. D.; Yang, M.; Lee, B.; Santos, A.; Podsiadlo, P.; Tang, Z.; Glotzer, S. C.; Kotov, N. A. Self-assembly of self-limiting monodisperse supraparticles from polydisperse nanoparticles. *Nat. Nanotechnol.* **2011**, *6* (9), 580–587.
- (58) He, M.; Gales, J. P.; Ducrot, É.; Gong, Z.; Yi, G.-R.; Sacanna, S.; Pine, D. J. Colloidal diamond. *Nature* **2020**, *585* (7826), 524–529.
- (59) Désert, A.; Hubert, C.; Fu, Z.; Moulet, L.; Majimel, J.; Barboteau, P.; Thill, A.; Lansalot, M.; Bourgeat-Lami, E.; Duguet, E.; Ravaine, S. Synthesis and site-specific functionalization of tetravalent, hexavalent, and dodecavalent silica particles. *Angew. Chem., Int. Ed.* **2013**, 52 (42), 11068–11072.
- (60) Tanjeem, N.; Chomette, C.; Schade, N. B.; Ravaine, S.; Duguet, E.; Tréguer-Delapierre, M.; Manoharan, V. N. Polyhedral plasmonic nanoclusters through multi-step colloidal chemistry. *Mater. Horiz.* **2021**, *8* (2), 565–570.
- (61) He, J. Y.; Zhang, Z. L.; Kristiansen, H.; Redford, K.; Fonnum, G.; Modahl, G. I. Crosslinking effect on the deformation and fracture of monodisperse polystyrene-co-divinylbenzene particles. *eXPRESS Polym. Lett.* **2013**, 7 (4), 365–374.
- (62) Cheong, F. C.; Kasimbeg, P.; Ruffner, D. B.; Hlaing, E. H.; Blusewicz, J. M.; Philips, L. A.; Grier, D. G. Holographic characterization of colloidal particles in turbid media. *Appl. Phys. Lett.* **2017**, *111* (15), 153702.
- (63) Israelachvili, J. N.; Adams, G. E. Measurement of forces between two mica surfaces in aqueous electrolyte solutions in the range 0–100 nm. *J. Chem. Soc., Faraday Trans. 1* **1978**, *74*, 975–1001.
- (64) Gutsche, C.; Keyser, U. F.; Kegler, K.; Kremer, F.; Linse, P. Forces between single pairs of charged colloids in aqueous salt solutions. *Phys. Rev. E* **2007**, *76* (3), 031403.
- (65) Damasceno, P. F.; Engel, M.; Glotzer, S. C. Crystalline assemblies and densest packings of a family of truncated tetrahedra and the role of directional entropic forces. *ACS Nano* **2012**, *6* (1), 609–614.
- (66) Zhang, K.; Chen, H.; Chen, X.; Chen, Z.; Cui, Z.; Yang, B. Monodisperse silica-polymer core-shell microspheres via surface

- grafting and emulsion polymerization. *Macromol. Mater. Eng.* 2003, 288 (4), 380–385.
- (67) Zerrouki, D.; Baudry, J.; Pine, D.; Chaikin, P.; Bibette, J. Chiral colloidal clusters. *Nature* **2008**, *455* (7211), 380–382.
- (68) Turner, M. D.; Saba, M.; Zhang, Q.; Cumming, B. P.; Schröder-Turk, G. E.; Gu, M. Miniature chiral beamsplitter based on gyroid photonic crystals. *Nat. Photonics* **2013**, *7*, 801–805.
- (69) Turner, M. D.; Schröder-Turk, G. E.; Gu, M. Fabrication and characterization of three-dimensional biomimetic chiral composites. *Opt. Express* **2011**, *19* (10), 10001–10008.
- (70) Saba, M.; Hamm, J. M.; Baumberg, J. J.; Hess, O. Group theoretical route to deterministic Weyl points in chiral photonic lattices. *Phys. Rev. Lett.* **2017**, *119*, 227401.
- (71) Brakke, K. A. The Surface Evolver. Exp. Math. 1992, 1 (2), 141–165.
- (72) Berthier, J.; Brakke, K. *The Physics of Microdroplets*; Scrivener Publishing LLC/John Wiley & Sons: Salem, MA, 2012; pp 31–39, 112–140.
- (73) Lauga, E.; Brenner, M. P. Evaporation-driven assembly of colloidal particles. *Phys. Rev. Lett.* **2004**, 93 (23), 238301.
- (74) Lee, J. G.; Brooks, A. M.; Shelton, W. A.; Bishop, K. J. M.; Bharti, B. Directed propulsion of spherical particles along three dimensional helical trajectories. *Nat. Commun.* **2019**, *10*, 2575.
- (75) Wang, Z.; Wang, Z.; Li, J.; Cheung, S. T. H.; Tian, C.; Kim, S.-H.; Yi, G.-R.; Ducrot, E.; Wang, Y. Active patchy colloids with shape-tunable dynamics. *J. Am. Chem. Soc.* **2019**, *141* (37), 14853–14863.
- (76) Ma, Y.; Aulicino, J. C.; Ferguson, A. L. Inverse design of self-assembling diamond photonic lattices from anisotropic colloidal clusters. *J. Phys. Chem. B* **2021**, *125* (9), 2398–2410.
- (77) Parvez, N.; Zanjani, M. B. Synthetic self-limiting structures engineered with defective colloidal clusters. *Adv. Funct. Mater.* **2020**, 30 (34), 2003317.
- (78) Tanaka, S.; Nogami, D.; Tsuda, N.; Miyake, Y. Synthesis of highly-monodisperse spherical titania particles with diameters in the submicron range. *J. Colloid Interface Sci.* **2009**, 334 (2), 188–194.
- (79) Sun, J.; Gao, L.; Zhang, Q. Synthesizing and comparing the photocatalytic properties of high surface area rutile and anatase titania nanoparticles. *J. Am. Ceram. Soc.* **2003**, *86* (10), 1677–1682.
- (80) Wang, X.; Bai, L.; Liu, H.; Yu, X.; Yin, Y.; Gao, C. A unique disintegration—reassembly route to mesoporous titania nanocrystal-line hollow spheres with enhanced photocatalytic activity. *Adv. Funct. Mater.* **2018**, 28 (2), 1704208.